ACCEPTED JUNE 27, 2011
Preprint typeset using LaTeX style emulateapj v. 11/10/09

arXiv:1106.5445v2 [astro-ph.HE] 24 Oct 2011

THE 2009 OUTBURST OF MAGNETAR 1E 1547−5408: PERSISTENT RADIATIVE AND BURST PROPERTIES

P. SCHOLZ[1] & V. M. KASPI[1]

Accepted June 27, 2011

ABSTRACT

The magnetar 1E 1547−5408 recently exhibited two periods of outburst, beginning on 2008 October 3 and 2009 January 22. Here we present an analysis of the persistent radiative evolution and a statistical study of the burst properties during the 2009 outburst using the *Swift* X-ray Telescope (XRT). We find that the 1–10 keV flux increased by a factor of ~ 500 and hardened significantly, peaking ~ 6 hours after the onset of the outburst. The observed pulsed fraction exhibited an anti-correlation with phase-averaged flux. Properties of the several hundred X-ray bursts during the 2009 outburst were determined and compared to those from other magnetar outburst events. We find that the peaks of the bursts occur randomly in phase but that the folded counts that compose the bursts exhibit a pulse which is misaligned with the persistent pulse phase. We also report a correlation between burst hardness and flux. We compare the hardness-flux evolution of the persistent emission of both outbursts to those from other magnetars and find that although there does exist an overall trend, the degree of hardening for a given increase in flux is not uniform from source to source. These results are discussed in the context of previous results and within the magnetar model.

Subject headings: stars: neutron — pulsars: individual (1E 1547−5408, PSR J1550−5418, SGR J1550−5418) — X-rays: bursts — X-rays: general

1. INTRODUCTION

Originally classified as two distinct types of objects, anomalous X-ray pulsars (AXPs) and soft gamma repeaters (SGRs) are now generally accepted to be highly magnetized neutron stars, magnetars, with magnetic fields $B > 10^{14} - 10^{15}$ G (for reviews, see Woods & Thompson 2006; Mereghetti 2008). Magnetars differ from 'normal' rotation-powered pulsars in that their X-ray luminosities exceed the rate of energy released from their spin-down. They are believed to be powered by the decay of their magnetic fields. Another common property of magnetars is that they exhibit episodes of violent bursting activity. At one point thought to be only observed in SGRs, X-ray bursts in AXPs were first detected from 1E 1048.1−5937 in late 2001 (Gavriil et al. 2002). Bursts have since been detected in several other AXPs (Kaspi et al. 2003; Woods et al. 2005; Krimm et al. 2006; Gavriil et al. 2009).

1E 1547−5408 was first discovered as an X-ray source by the *Einstein* satellite (Lamb & Markert 1981). It was identified only recently as a magnetar by Gelfand & Gaensler (2007) based on its X-ray spectrum and infrared flux, as well as its possible association with the supernova remnant G327.24−0.13. Pulsed radio emission was detected by Camilo et al. (2007) at a period of ∼2 s, the shortest period of all known magnetars[2]. An *XMM-Newton* observation in 2007 showed a significant flux enhancement from what was previously measured (Halpern et al. 2008), thus revealing that an X-ray outburst event had occured between 2006 and 2007. Another outburst event occured on 2008 October 3 and was detected by the *Swift* (Israel et al. 2010) and *Fermi* (Kaneko et al. 2010) satellites. 1E 1547−5408 entered yet another active phase on 2009 January 22 when hundreds of bursts were detected by *Swift*, *INTEGRAL*, and *Fermi*. Tiengo et al. (2010) report the appearance of dust scattering rings around 1E 1547−5408 after the 2009 burst in follow-up observations with *XMM-Newton* and *Swift*. The energy released by the event causing the rings was estimated to be $10^{44} - 10^{45}$ ergs. From these rings, a distance to the source was determined to be 3.9 kpc. Ng et al. (2011) report on *Chandra* observations beginning ∼ 2 days following the outburst. They note a lack of spectral variation during the flux decay as well as an anti-correlation between pulsed fraction and phase-averaged flux.

The origin and flux evolution of magnetar outbursts are not presently well understood (but see Perna & Pons 2011), and the sample of observed outbursts is still relatively small (for a review, see Rea & Esposito 2011). Hence, it is important for each magnetar outburst to be promptly observed and studied. The magnetar model suggests that outbursts are a result of magnetospheric twists of the magnetic field structure following some form of internal energy or stress release (Thompson et al. 2002; Beloborodov 2009), which predicts a correlation between hardness and X-ray flux in magnetar outbursts. Indeed a universal relationship between flux increase and spectral hardening might be expected, if not from source to source, at least for individual sources. Also, the origin and physics of X-ray bursts from magnetars are poorly understood. Bursts have been proposed to be magnetospheric in origin (Lyutikov 2003) as well as originating from stresses in the crust of the neutron star (Thompson & Duncan 1995). Detailed statistical studies of magnetar bursts can help determine their proper-

---

[1] Department of Physics, Rutherford Physics Building, McGill University, 3600 University Street, Montreal, Quebec, H3A 2T8, Canada

[2] see the McGill SGR/AXP Online Catalog, http://www.physics.mcgill.ca/∼pulsar/magnetar/main.html

ties for comparison with model predictions, yet have only been done for three sources thus far (Göğüş et al. 2001; Gavriil et al. 2004).

This paper presents the results of an analysis of the persistent emission from the 2009 event as well as a statistical study of the bursts using observations from *Swift*. The burst study will focus primarily on bursts from the 2009 outburst since the number (~ 400) is much higher than in the 2008 event, in which 8 bursts were detected by *Swift* (Israel et al. 2010). A summary of the observations is presented in §2. The analysis performed on the data as well as the results for the persistent emission are reported in §3.1. The analysis and results for the burst study are presented in §3.2. The results and their possible physical interpretations are discussed in §4. Finally, our findings are summarized in §5.

2. OBSERVATIONS

The data presented in this paper were obtained using the X-Ray Telescope (XRT) (Burrows et al. 2005) on the *Swift* satellite. The XRT uses Wolter-I optics and an *XMM-Newton*/EPIC MOS CCD detector to provide rapid imaging and spectra of X-ray transients in the 0.5–10 keV energy range. During the 2008 outburst of 1E 1547−5408, the *Swift* Burst Alert Telescope (BAT) triggered at 09:28:08 UT on 2008 October 3 and *Swift* promptly slewed to the source position. The XRT began taking observations 99 s after the trigger. On 2009 January 22, the BAT triggered at 01:32:41 UT and the first XRT observation began ∼50 min later. Table 1 shows a summary of the observations following the 2009 outburst event as well as two observations preceding the outburst. The observations following the 2008 outburst were previously presented by Israel et al. (2010); here we focus on the 2009 event.

Cleaned data products in both windowed-timing (WT) and photon-counting (PC) modes were obtained from the HEASARC *Swift* Archive. Data were reduced to the barycentre using the position of 1E 1547−5408, $15^{\mathrm{h}}50^{\mathrm{m}}54\overset{\mathrm{s}}{.}11$, $-54°18'23\overset{''}{.}7$ (Camilo et al. 2007). For WT mode, a source region consisting of a 40-pixel-long strip centered on the pulsar position was extracted. A background region of the same size was extracted on a source-free position away from 1E 1547−5408. For the PC mode data, an annulus with outer radius 20 pixels and 4 pixel inner radius was extracted for the source, and an annular region of 20 pixel inner radius and 50 pixel outer radius was used for the background. The 4 pixel inner region was excluded to avoid pileup.

3. ANALYSIS AND RESULTS

3.1. *Persistent flux evolution*

In order to investigate the behavior of the persistent flux of 1E 1547−5408 during the 2009 outburst, the observations were fitted with spectral models. Spectra were extracted from the event lists using `xselect`. Spectral fitting was performed using the XSPEC[3] package version 12.6. The spectra were grouped with a minimum of 20 counts per energy bin. Ancillary response files were created using the FTOOL `xrtmkarf` and the standard spectral redistribution matrices from the *Swift* CALDB were used. Bursts were then removed from the observations using the method described in §3.2.

The first two observations following the BAT trigger were split into shorter intervals ∼2 ks in length, since the spectral properties were evolving rapidly during that time. These split observations occured during the first day of the outburst when the dust scattering rings (Tiengo et al. 2010) were not fully resolved by the *Swift* XRT. For these observations, the radiative properties of the source cannot be simply disentangled from the delayed emission from the dust scattering rings (A. Tiengo & P. Esposito, private communication). Appropriate modelling of this is currently under investigation (Tiengo et al., in preparation) but beyond the scope of our work. Following the first day after the outburst, the dust scattering rings were outside of the extraction region and so those observations are not affected by dust scattering.

The spectra were fitted with a photoelectrically absorbed blackbody with an added power-law component. To determine N_H, we fit observations having an exposure time greater than 3 ks jointly with a single N_H. The parameters kT, Γ and their normalizations were allowed to vary in these fits. This resulted in $N_H = 3.24(5) \times 10^{22}$ cm^{-2} which is consistent with the value of $3.1^{+0.7}_{-0.8} \times 10^{22}$ cm^{-2} reported in Gelfand & Gaensler (2007), though is somewhat lower than the value of $4.1(1) \times 10^{22}$ cm^{-2} measured by Ng et al. (2011). All the *Swift* observations were subsequently fit with the column density fixed to our best-fit value. The 2008 data have been previously presented by Israel et al. (2010), whose results are generally consistent with those of our analysis for the same time period, so they will not be presented here. Figure 1 shows the results of fitting of the observations following the 2009 outburst. The split observations, affected by dust scattering, are the first 10 data points in Figure 1 following the trigger, and so should be regarded with caution. The two observations preceding the outburst were fit with only a blackbody and no power-law component. This is because the power-law index could not be constrained due to a paucity of counts. The fits in general were excellent; the goodness-of-fit statistic χ^2_ν ranged between 0.61 and 1.48 with a mean of 1.06.

The peak of the persistent emission occured ∼6 hr after the BAT first triggered on 1E 1547−5408 in 2009 January. The peak was almost 3 orders of magnitude higher in flux than the pre-outburst emission. This was accompanied by a hardening of the spectrum in the 1-10 keV band, as can be seen in the falling spectral index and rising kT. After the peak, the spectral index softened and kT fell as the flux dropped. To characterize the flux decay of the outburst, a power law decay was fit to the data following the first day of the outburst. The first day was not included as the source decay is superimposed by delayed emission from the dust scattering rings. The power law decay is descibed by $F = A(t - t_0)^\alpha$, where F is the unabsorbed flux, A is the normalization, α is the power-law index, and t_0 is the time of the BAT trigger. The decay was described by a power-law with an index of -0.24 ± 0.02. Although the χ^2_ν/ν of the fit was 4.1/23, a power-law model fit the data much better than an exponential decay. To determine the blackbody radius of the emitting region as shown in Figure 1, a distance of

---

[3] http://xspec.gfsc.nasa.gov

3.91 ± 0.07 kpc from Tiengo et al. (2010) was assumed.

To measure pulsed fractions and fluxes, the burst-removed time series (see §3.2) were folded at the rotational ephemeris derived from contemporaneous *RXTE* observations of 1E 1547−5408 (Dib et al. 2011). Specifically, we used spin frequency $\nu = 0.48259615(3)$ Hz, with frequency derivative $\dot{\nu} = -5.12(2) \times 10^{-12}$ s^{-2} at reference epoch MJD 54854.0 or 2009 January 23. The pulsed flux was calculated using an RMS method according to the formula in Dib et al. (2008), with 7 harmonics. The pulsed fraction was determined by dividing the pulsed flux by the phase-averaged flux. A pulsed flux and fraction were measured for each WT observation with an exposure time > 3 ks for which the ephemeris was valid. As seen in Figure 1, the pulsed fraction decreased as the flux increased. After ∼40 days, the pulsed fraction had not yet recovered to its pre-burst level of ∼0.25.

The pulsed flux evolution around both the 2008 and 2009 outburst events is presented in Figure 2. The *Swift* data confirm the evolution that is observed in the *RXTE* data which are presented briefly in Ng et al. (2011) and in detail in Dib et al. (2011). The pulsed flux enhancement ∼11 days following the initial trigger of the 2008 event, although not noted by Israel et al. (2010), is clearly present in the *Swift* data. Thus, the 2009 event showed a much smaller increase in pulsed flux than did the 2008 event, while the opposite is true of the total flux.

Figure 3 shows an anti-correlation between pulsed fraction and unabsorbed flux. It includes observations from both the 2008 and 2009 outbursts. Ng et al. (2011) present this trend using *Chandra* and *XMM* data as well as the burst-removed *Swift* data presented in this paper.

3.2. *X-Ray Bursts*

Bursts were identified in a manner similar to that described in Gavriil et al. (2004). The event lists were binned at a 1/16 s time resolution and a mean number of counts per bin was calculated for each Good Timing Interval (GTI). The number of counts in each bin, n_i, was compared to the GTI mean counts, λ, according to the probability P_i of n_i occuring randomly,

$$P_i = \frac{\lambda^{n_i} e^{-\lambda}}{n_i!}. \tag{1}$$

Time bins that had $P_i \leq 0.01/N$, where N is the total number of time bins in the GTI being searched, were identified as part of a burst. Since the mean number of counts in a GTI can be overestimated due to contamination from bursts in other time bins, the procedure above was repeated iteratively, each time removing the bins that were identified as containing bursts, until no further bursts were identified. The above procedure was then repeated for 1/32 s and 1/64 s time resolutions to improve sensitivity to bursts of different durations.

Since several bins identified with bursts can be part of the same burst, a burst was defined by its peak. The peak of a burst was determined by first finding the minimum time to accumulate 10 counts, using unbinned event data. The midpoint of the time spanned by these 10 counts was defined as the peak. A search for a peak was done within 0.5 s on each side of an identified bin. This definition of burst peak is independent of binning and, for bursts with durations shorter than 1 s, will merge all of the identified bins into a single burst. Bursts within 1 s of each other that were merged into a single burst were identified when selecting the background (see below) and their properties were measured separately.

Once identified, to remove the bursts from the event lists, the lists were divided into full periods of the pulsar, starting with the first event of the observation as a reference point. The periods that contained bursts were identified and all counts which arrived in that interval were removed from the event list. This was done to ensure equal exposure to all pulse phases in the pulse profile.

3.2.1. *Burst Statistics*

For each burst, a fluence, T_{90}, rise time (t_r), and fall time (t_f) were measured with the same analysis as in Gavriil et al. (2004), using the unbinned event data. The fluence was determined by first measuring a background count rate in hand-picked regions on either side of the burst. The background region by default was between 1 s and 2 s from the burst peak to either side of the burst, but was manually adjusted for most bursts in order to avoid contamination from other nearby bursts. The cumulative background-subtracted counts were then fit with a step function, using data point from the hand-picked background region. The height of the step function in counts corresponds to the fluence of the burst. The T_{90} duration of the burst is the time between when 5% and 95% of the fluence has been accumulated. The burst rise and fall times were determined using a maximum likelihood fit to a piecewise function with an exponential rise and an exponential decay. Peak fluxes in counts per second were determined by passing a 62.5 ms boxcar integrator through a 250 ms interval (4 boxcar widths) centered on the burst peak. The highest count rate measured by the integrator was defined to be the peak flux.

In total, for the 2009 outburst, 424 bursts were identified in 86 ks of observations from 2009 January 22 to 2009 September 30 using 1/16 s time resolution. Thirteen additional bursts were identfied using the 1/32 s and 1/64 s time resolutions for a total of 437 bursts. Of those identified, 34 had too few counts to permit a reliable measure of fluence, and for 32, the exponential rise and decay were not successfully fit. For 64 of the bursts, properties could not be measured because they were too close to another burst to allow a reliable background estimate between them. Four bursts were too close to the edge of a GTI to calculate a background count rate. In summary, 303 bursts could be fully analysed and only these 2009 bursts will be considered henceforth. Examples of different bursts are shown in Figure 4. Only two bursts were found in the XRT observations of the 2008 event; their properties were similar to those during the 2009 outburst.

Figure 5 shows the distributions of the burst properties, grouped in logarithmic bins. The T_{90}, rise time, fall time, and the ratio of rise to fall time distributions have been fit with log-normal distributions using maximum likelihood fitting. The T_{90} distribution has a mean of 305 ms and a range for one standard deviation of 140 - 662 ms. For the rise time distribution, we find a mean of 39 ms and a range for one standard deviation of 14 - 109 ms. For the distribution of fall times, we find a mean of 66 ms and a range of 24 - 182 ms for one standard deviation. The mean of the t_r/t_f distribution is 0.59 with a range for one standard deviation of 0.21 - 1.66. A summary of the measured quantities is provided in Table 2. There we also provide these quantities, when available, for the three other sources for which such statistical analyses have been done. We note in particular that the average burst duration for 1E 1547−5408 is longer than for all others measured thus far. This result is further discussed in §4.2.

Figure 6 shows the fluence and peak flux distributions, in counts and counts per second, respectively, which have been fitted with a power law using a least-squares method. For low fluences or peak fluxes, the number is underestimated since the burst detection algorithm is less sensitive to these bursts. Therefore, some of the points with low fluence or peak flux were not included in the fits. The best-fit power-law index for the fluence distribution is -0.6 ± 0.1. For the peak flux distribution, the power-law index is -0.34 ± 0.12. This index is quite shallow and, despite the omission of the first two points in the fit, may still be affected by the bias in the burst search.

For other AXPs, there is evidence that bursts tend to arrive on pulse (e.g. Gavriil et al. 2002, 2004). For 1E 1547−5408 this does not seem to be the case, as burst peaks are distributed randomly in phase (see Fig. 7a). This is similar to what is observed in SGRs 1806−20 and 1900+14 (Palmer 1999, 2002). However, when the individual photon arrival times that are part of bursts are folded, a strong pulse is observed. The peak of this 'pulse', shown in Figure 7b, is not aligned with the peak of the quiescent pulse profile. Figure 7e presents this quiescent pulse profile obtained using the burst-removed data. Since the pulsed fraction of the first two observations following the 2009 BAT trigger is significantly lower and the persistent flux is significantly higher than in the subsequent observations, including them in the profile reduces the pulse amplitude. Thus, in order to better show the persistent pulse profile, Figure 7e does not include those first two observations. In order to determine whether the burst count pulse was dominated by a handful of bright bursts, the 15 brightest bursts were removed and the counts were refolded. The profile did not change significantly and still displayed a pulse at a similar phase.

Panels c and d of Figure 7 separate the symmetric bursts from slow-fall bursts. Symmetric bursts were defined as bursts with $0.5 < t_r/t_f < 2$. Bursts with t_f greater than $2\,t_r$ were defined as slow-fall bursts. Of the 303 well measured bursts, 158 were classified as symmetric and 116 as slow falls. The remainder, 29 bursts, were those with rise times greater than twice their fall times. Curiously, the folded slow-fall burst counts exhibit a much stronger pulse than do the folded symmetric burst counts, with a $\chi^2_\nu = 43$ for the null hypothesis, compared to $\chi^2_\nu = 6$ for the folded symmetric bursts. This symmetric/slow-fall definition is somewhat arbitrary and these two classes of bursts are by no means distinct populations. We use this distinction only to demonstrate that the more symmetric bursts tend to be more pulsed than those that are less symmetric.

3.2.2. *Burst Spectroscopy*

Spectra within the T_{90} interval of each burst peak were extracted and grouped with 20 counts per bin. Background spectra were taken from 1 min on either side of the burst peak extracted from the burst-removed event data. The 46 bursts with fluences over 200 background-subtracted counts were fitted with a photoelectrically absorbed power law with N_H fixed to 3.24×10^{22} cm^{-2} as measured from the fit to the persistent emission (see §3.1). The spectra were fitted using XSPEC. The mean of the measured spectral indices of the bursts was found to be $\Gamma = 0.17$, with a standard deviation of 0.33, where $N(E) \propto E^{-\Gamma}$. Fitting with more complicated models was attempted, but parameters could not be successfully constrained because of the low number of counts. As shown in Table 2, the average Γ we measure is significantly harder than that measured in the only other magnetar outburst for which the value is reported. This is discussed further in §4.2.

In order to determine the effect of pileup on the bursts, power-law spectra were fit to the two bursts with the highest peak flux while excluding a central region ranging from 1 to 15 pixels in radius. The power-law indices from the fits were plotted against radius of exclusion region as per the prescription of Romano et al. (2006). The power-law index did not change significantly as a function of exclusion radius. Hence we concluded that the bursts were not significantly affected by pileup.

In order to probe the relation between hardness and fluence for the bursts, hardness ratios were determined for each burst by measuring fluences in the 0.5–4 keV and 4–10 keV bands. No significant correlation between 0.5–4 keV/4–10 keV hardness and fluence was observed for bursts from 1E 1547−5408. For the 46 most fluent bursts, there was also no observed correlation between the 0.5–4 keV/4–10 keV hardness or the spectral index of the power-law fit and the fluence. The lack of a detection of the correlation between hardness and fluence in the *Swift* data may be due to the limited spectral range of the XRT (0.5–10 keV). However, an anti-correlation between power-law index and average flux over T_{90} from the spectral fits was observed (Fig. 8). This is consistent with a correlation between the hardness and the magnitude of a burst.

Spectral features in magnetar bursts have been reported for some sources (Strohmayer & Ibrahim 2000; Ibrahim et al. 2002; Gavriil et al. 2002; Ibrahim et al. 2003; Woods et al. 2005; Gavriil et al. 2009; Kumar & Safi-Harb 2010), although most of the features have been discovered above 10 keV. The individual burst spectra for 1E 1547−5408 showed no evidence for any spectral features in the 1-10 keV range. Since spectral features may be masked by the low count rates in the individual spectra, we combined the burst spectra into a single average spectrum. The burst and background spectra and response filestend to bere combined using the FTOOL `addspec`. Spectral bins were grouped with a minimum of 20 counts per bin. The average spectrum was fit with a blackbody, a power law, a blackbody with an added power law, and a Comptonized blackbody; all four models were photoelectrically absorbed. All of the models gave acceptable fits with $\chi^2_\nu \sim 1$; thus, no significant spectral features were observed in any of the residuals.

Fluences and peak fluxes in counts and counts per second, respectively, were converted into cgs units using the results of the spectral fits. The fluxes from the power-law fits were multiplied by the burst durations and compared to the fluences measured in counts. The proportionality constant between the two was determined to be 2.23×10^{-10} ergs cm^{-2} counts^{-1}. In using this single conversions factor between counts and ergs cm^{-2} we are effectively assuming an average spectral model for the bursts which is not generally true. The conversion from counts to cgs units in reality is different from burst to burst depending on their spectra. Values in cgs units, using this single conversion factor, are indicated on the top axes of the fluence and peak flux distributions in Figure 6.

4. DISCUSSION

We have presented *Swift* XRT observations of the 2008 and 2009 outburst events of 1E 1547−5408. In particular, we considered the behavior of this source's persistent flux in its 2009 outburst, which was qualitatively different from that in 2008. Specifically, the 2009 event showed a much smaller increase in pulsed flux than in 2008, while the opposite is true of the total flux. In this work, we have shown that for the 2009 outburst, the source spectrum became harder (though the exact degree of hardening is presently difficult to know, due to the contaminating dust scattering) as the flux increased after the initial trigger, and we found an anti-correlation between the pulsed fraction and the flux.

We have also presented a detailed study of the several hundred X-ray bursts detected by *Swift* following the 2009 event. Noteworthy results we have found include a correlation between burst flux and hardness. We also note that burst counts tend to contribute very significantly to the pulsed fraction, even if the phases of burst peaks are randomly distributed in pulse phase.

Next we discuss our results in the context of the magnetar model, as well as in comparison with those for other similar outbursts.

4.1. *Persistent Flux*

Figure 1 shows that as the X-ray flux increased, the blackbody temperature increased and the power-law index decreased during the 2009 outburst. Such a hardness/flux correlation was seen also in the 2008 outburst (Israel et al. 2010) and ubiquitously in other magnetar outbursts (e.g. Kaspi et al. 2003; Woods et al. 2004; Israel et al. 2007). In the case of 1E 1547−5408, however, we regard the precise values of kT and Γ as shown in Figure 1 on the first day after the outburst with caution, as they are very likely biased by dust scattering. The hardness/flux correlation for this outburst on the day of the trigger is likely to be robust, since dust scattering softens photons. However, note that if the dust scattering rings are caused by a burst that is much harder than, and separate from, the persistent emission, the dust scattering could effectively cause the overall emission to harden in relation to the true persistent emission.

The thermal emission of magnetars, in the twisted magnetosphere model (Thompson et al. 2002), has as its origin heating from within the star, due to the decay of the strong internal magnetic field. The resulting thermal surface photons are thought to be scattered by currents in the atmosphere, resulting in a Comptonized blackbody-like spectrum which is often modelled with a blackbody plus a power law (Lyutikov & Gavriil 2006). The magnetospheric currents are present due to 'twists' in the field structure, either global (Thompson et al. 2002), or, more likely, in localized regions (Beloborodov 2009). In either case, the current strength, hence degree of scattering, increases with increasing twist magnitude. Moreover, return currents provide an additional, external source of surface heating in addition to the internal source. The increase in flux during a magnetar outburst is thus theorized to be caused by an internal heat-releasing event that may significantly increase the surface temperature (see, for example, Özel & Guver 2007), further twist the magnetospheric field, and increase the external return-current heating. Thus, a correlation between hardness and flux is generically expected in the twisted-magnetosphere model (Lyutikov & Gavriil 2006), in agreement with observations of 1E 1547−5408 and other magnetars.

It is interesting to compare the hardness/flux correlations seen for 1E 1547−5408 with those observed for other magnetars to see if there exists a universal relationship between increase in X-ray flux and hardness, as might be expected in the above scenario. Figure 9 shows the fractional increase in the 4–10/2–4 keV hardness ratio determined from fluxes as a function of 2–10 keV unabsorbed flux fractional increase for six different magnetar outbursts in four different magnetars. We chose to consider a flux hardness ratio as a measure of hardness (rather than e.g. power-law index) as it is defined independent of spectral model, and also is instrument-independent. In order to determine the hardness of each source, spectral model parameters from the literature were compiled and input to XSPEC. The 4–10 keV and 2–4 keV fluxes were then determined using the XSPEC `flux` command and the hardness was calculated from their ratio. For references that did not report a 2–10 keV unabsorbed flux, one was determined using XSPEC using the reported model paramenters. As is clear from the Figure, an overall trend is apparent, although there is significant variation from source to source. For example, for similar flux enhancements over the quiescent level, 1E 2259+586 became much harder than did 1E 1048.1−5937, with the behavior of 1E 1547−5408 lying somewhere in between. Thus, though Figure 9 demonstrates that a hardness/flux correlation is indeed generically observed, there does not appear to exist a universal law linking the degree of flux increase over the quiescent level with the degree of flux hardening. This observation will require accommodation in any detailed model of magnetar outburst emission.

As shown in Figure 3, the flux of 1E 1547−5408 was anti-correlated with the pulsed fraction. While immediately preceding the 2009 outburst the pulsed fraction was over 20% (Fig. 1), immediately afterward, it dropped to nearly negligible levels in the 1–10 keV range, likely due to the emission being dominated by the scattered emission from the dust scattering rings. However, following the first day, the pulsed fraction was still significantly lower than the preburst pulsed fraction. This anti-correlation between pulsed fraction and flux is presented with the addition of *Chandra* and *XMM-Newton* data in Ng et al. (2011), who suggest it could be due to an increase in the emitting area of a thermal hot spot, which would cause the emission to be observable during a greater portion of the phase of the pulsar. We note that both correlations (Gotthelf et al. 2004; Zhu et al. 2008) and anti-correlations (Israel et al. 2007; Tam et al. 2008) between pulsed fraction and flux have been observed in magnetar outbursts. Different behaviors can result depending on the location of the emission region and the viewing geometry. Although detailed modeling of spectral, pulse morphology and pulsed flux changes during magnetar outbursts is beyond the scope of this paper, recent attempts at unified modelling of magnetar surface and magnetosphere emission geometries and emission mechanisms (Albano et al. 2010) could in principle use data like ours to constrain the hot spot location and size. This seems to us to be a good future avenue for investigation.

Interestingly, Kaneko et al. (2010) report a ∼55% pulsed fraction at ∼100 keV as observed by *Fermi* GBM ∼30–40 minutes before the BAT trigger. They report that this is the first time that pulsations unrelated to a giant flare have been observed at ∼100 keV for an SGR[4]. However, AXPs have previously been shown to exhibit pulsations at ∼100 keV with pulsed fractions as high as 100% (e.g. Kuiper et al. 2006). Thus it is possible that the measured 55% actually decreased from a higher pulsed fraction leading up to the outburst event, i.e. the ∼100 keV pulsed fraction may have behaved similarly to that in the 1–10 keV band. Future hard X-ray telescopes with focusing optics, such as *NuSTAR*, will allow much easier measurements of the pulsed fraction of magnetars at high X-ray energies.

4.2. *Bursts*

Previous studies of SGR bursts have shown that their energies, and thus fluences, follow a power-law distribution $dN/dE \propto E^{-\alpha}$ with α equal to ∼5/3 (Cheng et al. 1996; Göğüş et al. 1999, 2000). It has been noted that this is similar to the Gutenberg-Richter law for earthquakes and to energy distributions of solar flares (Crosby et al. 1993; Lu et al. 1993). Both 1E 1547−5408 and 1E 2259+586 also follow this distribution. In this work, the fluence distribution of 1E 1547−5408 is found to have a power-law index of -0.6 ± 0.1 which corresponds to $dN/dE \propto E^{-1.6}$. Gavriil et al. (2004) find an α of 1.7 ± 0.1 for 1E 2259+586, similar to the values found for SGRs, further reinforcing the similarity in this particular behavior among AXPs and SGRs.

For the 2009 outburst, *INTEGRAL* observations which cover an energy range of > 80 keV, show different burst properties from those determined using the *Swift* XRT observations. Savchenko et al. (2010) report a 68-ms mean duration derived from a log-normal distribution with a scatter of 30 - 155 ms. This is much shorter than the 305-ms duration determined in this work (see Table 2). This discrepency may be due to the difference in energy coverage; perhaps bursts have different morphologies at different energies. However, the definition of duration used by Savchenko et al. (2010) differs from the T_{90} definition used here. Savchenko et al. (2010) define the burst duration as the time between the moment when the count rate rises above 5σ to when the count rate drops below 3σ. When applying their definition of duration to the bursts identified in our study, we find, for a log-normal distribution, a mean duration of 101 ms and a range for one standard deviation of 59 - 173 ms, closer to but still somewhat longer than their measurement, suggesting a possible energy dependence of burst duration. We do not, however, detect any significant difference in the durations measured using 0.5–10 keV counts with those measured using 2–10 keV counts.

The properties of bursts from the 2009 outburst event of 1E 1547−5408 are reminiscent of those from the outburst of 1E 2259+586 (Gavriil et al. 2004). Both have a significant number of short spikes like those found in SGRs, and a set of bursts with long pulsating tails like those found in burst studies of other AXPs. Although we do not find any bursts with long pulsating tails in the XRT observations, Savchenko et al. (2010) and Mereghetti et al. (2009) find two such bursts. These were not found in our analysis because *Swift* was not observing 1E 1547−5408 when they occured. Table 2 compares the properties of bursts from 1E 1547−5408 to those from outbursts from other magnetars. We note that the average durations of bursts from 1E 1547−5408 appear to be longer than for those in other sources. However, this could be an artifact as the burst properties for the other tabulated sources were determined with *RXTE*. The larger collecting area of *RXTE* allows it to detect bursts that are fainter than those *Swift* can detect. If faint, short bursts are missed by the XRT, the mean burst duration (as well as t_r and t_f) may be overestimated. Also, the energy range of RXTE (2–60 keV) probes higher energies and so differences may be due to the energy dependance of burst properties. A detailed statistical study of 1E 1547−5408 bursts with *RXTE* is needed to clarify this point.

Although *Swift* XRT is not ideal for probing the spectra of magnetar bursts, which have significant flux above 10 keV, we were still able to draw the following conclusions from our analysis. While we do not observe a hardness-fluence correlation for 1E 1547−5408, this could be due to our limited energy range. Indeed, there is a hint of a correlation between Γ and fluence, however is is not statistically significant. Note however that we do observe a significant Γ-flux correlation (Fig. 8). Savchenko et al. (2010), using *INTEGRAL* data of the 2009 outburst, find a correlation between burst hardness and count rate. Their hardness ratio is defined as the ratio between the Anti-Coincidence Shield (ACS) flux, which is sensitive to photons above 80 keV, and a 20-60 keV flux from the ISGRI instrument. This is also consistent with a correlation between hardness and burst magnitude for 1E 1547−5408. Gavriil et al. (2004) also find a correlation between hardness and fluence for 1E 2259+586. For the SGRs, on the other hand, an anti-correlation between hardness and fluence has been observed (Göğüş et al. 1999, 2000). Table 2 also shows that the 1E 1547−5408 bursts from *Swift* are much harder than those from 1E 2259+586. In light of the observed hardness-fluence correlation in AXP bursts, this is not a suprising result. The 28 most fluent bursts from 1E 2259+586 for which spectral indices were measured, have fluences of $\sim 10^{-9} - 10^{-8}$ erg cm^{-2} (Gavriil et al. 2004). This is to be compared with the 46 most fluent bursts for which Γ was measured here for 1E 1547−5408, that span a fluence range of $\sim 10^{-8} - 10^{-7}$ erg cm^{-2}. This may account for the harder average spectral index for bursts from 1E 1547−5408.

---

[4] Note that Kaneko et al. (2010) use the designation SGR 1550−5418 for 1E 1547−5408.

In the magnetar model, two mechanisms have been suggested for producing magnetar bursts. Thompson & Duncan (1995) suggest that stresses due to the strong magnetic fields present inside magnetars are able to crack the crust of the neutron star. This cracking releases a plasma fireball into the magnetosphere. The strong magnetic fields can hold the fireball above the fracture site. The suspended fireball can heat the surface thus causing an extended cooling tail. Since the strongest surface fields are located near the polar caps, these fracture events would occur preferentially near the poles which would result in an observed phase dependence of the bursts. Another mechanism, proposed by Lyutikov (2003), suggests that bursts are caused by reconnection events initiated by the development of a tearing mode instability in the magnetically dominated relativistic plasma in the magnetosphere. In this case, bursts occur randomly in phase. This mechanism should also produce shorter more symmetric bursts than in crustal fracture. Lyutikov (2003) states that the hardness-fluence anticorrelation found in SGRs is consistent with magnetic reconnection. For the surface-cooling model, the opposite is expected. As discussed by Lyutikov (2003), both mechanisms could easily be at work.

Woods et al. (2005) suggested that observationally, there are two types of magnetar bursts. Type A bursts are nearly symmetric and are typical of SGR bursts. Type B bursts have been observed in AXPs and are characterized by a short spike followed by a long tail, typically much longer than the rotational period of the pulsar. Pulsations have been observed in these tails. Since the Type B bursts observed in AXPs occur preferentially in phase and exhibit a hardness-fluence correlation, and the Type A bursts in SGRs are distributed randomly in phase and have a hardness-fluence anti-correlation, Woods et al. (2005) suggest the magnetic reconnection mechanism for type A bursts and the surface-cooling model for Type B bursts.

For 1E 1547−5408, none of the bursts detected by *Swift* XRT could be classified as Type B. However, the two bursts with long pulsating tails found in *INTEGRAL* data by Savchenko et al. (2010) and Mereghetti et al. (2009) have typical Type B morphology. For the bursts in this work, over half of the bursts were classified as symmetric, which nominally corresponds to Type A (see top-right panel of Figure 4 for example). About 40% of the bursts were classified as slow-fall bursts, which are actually closer to Type A in morphology than Type B, although they are not very symmetric. Thus, the bursts from 1E 1547−5408 are not easily classified into Types A and B as described by Woods et al. (2005). Moreover, for both the symmetric and slow-fall bursts, the folded photon arrival times exhibited a clear phase dependence, although for the slow-fall bursts this ‘pulse’ is much stronger. That the symmetric bursts show some pulse modulation is suggestive of a difference with ‘classical’ Type A bursts, or that pulse phase analyses of the latter should be attempted using all burst counts, as they too may be pulsed. That the burst counts are pulsed indicates that burst emission comes from a preferred region in rotational phase, be it on or near the surface or high in the magnetosphere, even if the burst peaks arrive randomly in phase. The offset between the burst counts pulse peak and the persistent pulse peak seen when comparing Figures 7b and 7e demonstrates that the preferred burst emission region has location and geometry similar to, but distinct from, that producing the persistent pulsations.

The total energy released in the *Swift*-detected bursts was $\sim 1 \times 10^{40}$ erg in the 1-10 keV range. This is much lower than the 1-10 keV energy released from the persistent emission between 2009 January 22 and 2009 September 30 of $\sim 9 \times 10^{41}$ erg. For reference, the energy released from the spin-down in that same period is $\sim 5 \times 10^{40}$ erg. Woods et al. (2004) find that for SGRs, the energy released in the bursts is higher than that released in the persistent emission, but for 1E 2259+586, the opposite is true. In this regard, the 2009 outburst of 1E 1547−5408 is more like that of AXP 1E 2259+586.

5. CONCLUSIONS

We have presented an analysis of the persistent radiative evolution of the 2009 January outburst of 1E 1547−5408 from *Swift* XRT observations. We found that $\sim$ 6 hr after the 2009 BAT trigger the observed persistent 1–10 keV unabsorbed flux reached a peak of $\sim 8 \times 10^{-9}$ ergs cm^{-2} s^{-1}, an increase of more than 500 times the quiescent flux leading up to the outburst. This flux evolution is not due solely to the source; in the first day, there is also emission from dust scattering rings that is delayed emission from an energtic event near the onset of the outburst. There was significant spectral hardening at the outburst as seen in other magnetar outbursts. Note that the absence of spectral variation reported by Ng et al. (2011) is consistent with our results, as they missed the bulk of the spectal changes which occured in the first day of the outburst and their *Chandra* observations did not begin until the next day. The pulsed fraction showed an anti-correlation with the phase-averaged flux for both the previous 2008 and 2009 outbursts, with both sets of data following the same trend. We have compiled data from this and five other magnetar outbursts for four different sources and find a generic X-ray hardness/flux correlation overall, but with no clear universal quantitative relationship between the two.

We have also presented a detailed statistical analysis of the several hundred bursts detected during the 2009 event. The bursts do not easily fall into the Type A/Type B classification put forth by Woods et al. (2005). We found that the peaks of the bursts were randomly distributed in pulse phase, but that when the individual photon counts were folded at the pulsar ephemeris, a clear pulse was present. This phase dependence is stronger for those bursts with longer decays than rise times than for those bursts that are symmetric. We also report a correlation between burst hardness and burst flux.

In many ways, these observations yield more questions than answers. The range of observed phenomenology in magnetar outbursts seems to increase with each event, with few overall trends to assist in constraining models emerging. Nevertheless given the paucity of events studied in detail, we remain hopeful that through perserverence, eventually physical insight will emerge. The fast response of telescopes like *Swift* is crucial to this endeavor. For 1E 1547−5408, it allowed an analysis of the first day of the 2009 event. This is important as both the most significant spectral changes and the majority of the bursts occured within this period. This highlights the necessity of prompt response to magnetar outbursts in understanding their nature.

After submission of our manuscript, we became aware of the work by Bernardini et al. (2011) on the 2009 outburst of 1E 1547−5408 using *Swift* XRT data. A preliminary comparison of their results with ours shows general agreement. In particular their reported overall source behavior, namely spectral hardening correlated with flux, as well as pulsed fraction anti-correlated with flux and blackbody radius, are in broad agreement with our results. We further note that they omitted reporting on data taken with *Swift* XRT in the 24 hrs following the 2009 trigger, due to the difficulty in handling the dust-scattered emission (P. Esposito, A. Tiengo, private communication).

We are grateful to P. Esposito and A. Tiengo for sharing with us their preliminary work on modelling of the dust-scattered emission on the first day following the onset of the 2009 outburst. We thank A. Archibald, P. Lazarus, C.-Y. Ng, and S. Olausen for useful discussions. We thank R. Dib for providing an ephemeris and pulsed count rate measurements from *RXTE*. We thank P. Woods for helpful comments. V.M.K. holds the Lorne Trottier Chair in Astrophysics and Cosmology and a Canadian Research Chair in Observational Astrophysics. This work is supported by NSERC via a Discovery Grant, by FQRNT, by CIFAR, and a Killam Research Fellowship.

REFERENCES

Albano, A., Turolla, R., Israel, G. L., Zane, S., Nobili, L., & Stella, L. 2010, ApJ, 722, 788
Beloborodov, A. M. 2009, ApJ, 703, 1044
Bernardini, F., Israel, G. L., Stella, L., Turolla, R., Esposito, P., Rea, N., Zane, S., Tiengo, A., Campana, S., Gotz, D., Mereghetti, S., & Romano, P. 2011, A&A, in press; arXiv:1102.5419
Burrows, D. N., Hill, J. E., Nousek, J. A., Kennea, J. A., Wells, A., Osborne, J. P., Abbey, A. F., Beardmore, A., Mukerjee, K., Short, A. D. T., Chincarini, G., Campana, S., Citterio, O., Moretti, A., Pagani, C., Tagliaferri, G., Giommi, P., Capalbi, M., Tamburelli, F., Angelini, L., Cusumano, G., Bräuninger, H. W., Burkert, W., & Hartner, G. D. 2005, Space Sci. Rev., 120, 165
Camilo, F., Ransom, S. M., Halpern, J. P., & Reynolds, J. 2007, ApJ, 666, L93
Cheng, B., Epstein, R. I., Guyer, R. A., & Young, A. C. 1996, Nature, 382, 513
Crosby, N. B., Aschwanden, M. J., & Dennis, B. R. 1993, Solar Physics, 143, 275
Dib, R., Kaspi, V. M., & Gavriil, F. P. 2008, ApJ, 673, 1044
—. 2011, ApJ, submitted
Gavriil, F. P., Dib, R., & Kaspi, V. M. 2009, ApJ, submitted; arXiv:0905.1256
Gavriil, F. P., Kaspi, V. M., & Woods, P. M. 2002, Nature, 419, 142
—. 2004, ApJ, 607, 959
Gelfand, J. D. & Gaensler, B. M. 2007, ApJ, 667, 1111
Gotthelf, E. V. & Halpern, J. P. 2007, ApJS, 308, 79
Gotthelf, E. V., Halpern, J. P., Buxton, M., & Bailyn, C. 2004, ApJ, 605, 368
Göğüş, E., Kouveliotou, C., Woods, P. M., Thompson, C., Duncan, R. C., & Briggs, M. S. 2001, ApJ, 558, 228
Göğüş, E., Woods, P. M., Kouveliotou, C., van Paradijs, J., Briggs, M. S., Duncan, R. C., & Thompson, C. 1999, ApJ, 526, L93
Göğüş, E., Woods, P. M., Kouveliotou, C., van Paradijs, J., Briggs, M. S., Duncan, R. C., & Thompson, C. 2000, ApJ, 532, L121
Halpern, J. P., Gotthelf, E. V., Reynolds, J., Ransom, S. M., & Camilo, F. 2008, ApJ, 676, 1178
Ibrahim, A. I., Safi-Harb, S., Swank, J. H., Parke, W., Zane, S., & Turolla, R. 2002, ApJ, 574, L51
Ibrahim, A. I., Swank, J. H., & Parke, W. 2003, ApJ, 584, L17
Israel, G. L., Campana, S., Dall'Osso, S., Muno, M. P., Cummings, J., Perna, R., & Stella, L. 2007, ApJ, 664, 448
Israel, G. L., Esposito, P., Rea, N., Dall'Osso, S., Senziani, F., Romano, P., Mangano, V., Götz, D., Zane, S., Tiengo, A., Palmer, D. M., Krimm, H., Gehrels, N., Mereghetti, S., Stella, L., Turolla, R., Campana, S., Perna, R., Angelini, L., & de Luca, A. 2010, MNRAS, 408, 1387
Kaneko, Y., Göğüş, E., Kouveliotou, C., Granot, J., Ramirez-Ruiz, E., van der Horst, A. J., Watts, A. L., Finger, M. H., Gehrels, N., Pe'er, A., van der Klis, M., von Kienlin, A., Wachter, S., Wilson-Hodge, C. A., & Woods, P. M. 2010, ApJ, 710, 1335
Kaspi, V. M., Gavriil, F. P., Woods, P. M., Jensen, J. B., Roberts, M. S. E., & Chakrabarty, D. 2003, ApJ, 588, L93
Krimm, H., Barthelmy, S., Campana, S., Cummings, J., Israel, G., Palmer, D., & Parsons, A. 2006, The Astronomer's Telegram, 894
Kuiper, L., Hermsen, W., den Hartog, P. R., & Collmar, W. 2006, ApJ, 645, 556
Kumar, H. S. & Safi-Harb, S. 2010, ApJ, 725, L191
Lamb, R. C. & Markert, T. H. 1981, ApJ, 244, 94
Lu, E. T., Hamilton, R. J., McTiernan, J. M., & Bromund, K. R. 1993, ApJ, 412, 841
Lyutikov, M. 2003, MNRAS, 339, 623
Lyutikov, M. & Gavriil, F. P. 2006, MNRAS, 368, 690
Mereghetti, S. 2008, Astron. Astropys. Rev., 15, 225
Mereghetti, S., Götz, D., Weidenspointner, G., von Kienlin, A., Esposito, P., Tiengo, A., Vianello, G., Israel, G. L., Stella, L., Turolla, R., Rea, N., & Zane, S. 2009, ApJ, 696, L74
Ng, C., Kaspi, V. M., Dib, R., Olausen, S. A., Scholz, P., Güver, T., Özel, F., Gavriil, F. P., & Woods, P. M. 2011, ApJ, 729, 131
Özel, F. & Guver, T. 2007, ApJ, 659, L141
Palmer, D. M. 1999, ApJ, 512, L113
—. 2002, Memorie della Societa Astronomica Italiana, 73, 578
Perna, R. & Pons, J. A. 2011, ApJ, 727, L51+
Rea, N. & Esposito, P. 2011, in High-Energy Emission from Pulsars and their Systems, ed. D. F. Torres & N. Rea (Springer ASSP), arXiv:1101.4472v1
Romano, P., Campana, S., Chincarini, G., Cummings, J., Cusumano, G., Holland, S. T., Mangano, V., Mineo, T., Page, K. L., Pal'Shin, V., Rol, E., Sakamoto, T., Zhang, B., Aptekar, R., Barbier, S., Barthelmy, S., Beardmore, A. P., Boyd, P., Burrows, D. N., Capalbi, M., Fenimore, E. E., Frederiks, D., Gehrels, N., Giommi, P., Goad, M. R., Godet, O., Golenetskii, S., Guetta, D., Kennea, J. A., La Parola, V., Malesani, D., Marshall, F., Moretti, A., Nousek, J. A., O'Brien, P. T., Osborne, J. P., Perri, M., & Tagliaferri, G. 2006, A&A, 456, 917
Savchenko, V., Neronov, A., Beckmann, V., Produit, N., & Walter, R. 2010, A&A, 510, A77+
Strohmayer, T. E. & Ibrahim, A. I. 2000, ApJ, 537, L111
Tam, C. R., Gavriil, F. P., Dib, R., Kaspi, V. M., Woods, P. M., & Bassa, C. 2008, ApJ, 677, 503
Thompson, C. & Duncan, R. C. 1995, MNRAS, 275, 255
Thompson, C., Lyutikov, M., & Kulkarni, S. R. 2002, ApJ, 574, 332
Tiengo, A., Vianello, G., Esposito, P., Mereghetti, S., Giuliani, A., Costantini, E., Israel, G. L., Stella, L., Turolla, R., Zane, S., Rea, N., Götz, D., Bernardini, F., Moretti, A., Romano, P., Ehle, M., & Gehrels, N. 2010, ApJ, 710, 227

Table 1
Summary of *Swift* XRT observations of the 2009 outburst of 1E 1547−5408

Sequence	Mode	Observation date	MJD (TDB)	Exposure time (ks)	Time since trigger (days)
00090007024	WT	2009-01-04	54835.0	3.3	−18.033
00090007025	WT	2009-01-12	54844.0	4.2	−9.066
00340573000	WT	2009-01-22	54853.1	6.1	0.035
00340573001	WT	2009-01-22	54853.4	9.2	0.321
00340923000	PC	2009-01-23	54854.6	1.7	1.575
00090007026	WT	2009-01-23	54854.7	8.2	1.657
00340986000	PC	2009-01-24	54855.2	2.9	2.110
00030956031	PC	2009-01-24	54855.3	2.5	2.195
00090007027	WT	2009-01-25	54856.1	3.3	2.990
00341055000	PC	2009-01-25	54856.1	4.0	3.065
00341114000	PC	2009-01-25	54856.9	4.6	3.851
00090007028	WT	2009-01-26	54857.1	3.5	3.987
00030956032	PC	2009-01-27	54858.1	6.2	4.996
00090007029	WT	2009-01-27	54858.4	1.8	5.330
00030956033	PC	2009-01-28	54859.2	5.1	6.143
00090007030	WT	2009-01-28	54859.9	1.9	6.811
00030956034	PC	2009-01-29	54860.0	5.9	6.941
00090007031	WT	2009-01-29	54860.7	2.2	7.614
00090007032	WT	2009-01-30	54861.5	2.9	8.476
00030956035	WT	2009-01-30	54861.7	3.0	8.677
00030956036	WT	2009-01-31	54862.1	3.0	9.076
00090007033	WT	2009-01-31	54862.8	2.5	9.687
00030956037	WT	2009-02-01	54863.5	2.0	10.476
00090007035	WT	2009-02-02	54864.6	4.1	11.548
00030956038	PC	2009-02-03	54865.5	5.9	12.424
00030956039	PC	2009-02-04	54866.7	6.1	13.637
00030956040	WT	2009-02-05	54867.2	6.1	14.101
00030956042	WT	2009-02-07	54869.3	1.7	16.189
00090007036	WT	2009-02-12	54874.1	4.6	21.056
00090007037	WT	2009-02-22	54884.5	4.6	31.431
00090007038	WT	2009-03-04	54894.5	3.9	41.408
00090007039	WT	2009-03-13	54904.0	4.1	50.912
00090007040	WT	2009-03-24	54914.8	4.2	61.763
00030956054	WT	2009-09-30	55104.5	3.3	251.428

Table 2
Burst statistics of magnetars

Magnetar	$\overline{T_{90}}$ (ms)	$\overline{t_r}$ (ms)	$\overline{t_f}$ (ms)	$\overline{\Gamma}$	B^a (10^{14} G)	P^a (s)	Reference
SGR 1806−20	161.8	-	-	-	21	7.6	Göğüş et al. (2001)
SGR 1900+14	93.4	-	-	-	7.3	8.0	Göğüş et al. (2001)
1E 2259+586	99.31	2.43	13.21	1.35	0.59	7.0	Gavriil et al. (2004)
1E 1547−5408	305	39	66	0.17	2.2	2.1	this work

[a] From the McGill AXP/SGR catalogue at http://www.physics.mcgill.ca/∼pulsar/magnetar/main.html

Woods, P. M., Kaspi, V. M., Thompson, C., Gavriil, F. P., Marshall, H. L., Chakrabarty, D., Flanagan, K., Heyl, J., & Hernquist, L. 2004, ApJ, 605, 378

Woods, P. M., Kouveliotou, C., Gavriil, F. P., Kaspi, M., V., Roberts, M. S. E., Ibrahim, A., Markwardt, C. B., Swank, J. H., & Finger, M. H. 2005, ApJ, 629, 985

Woods, P. M. & Thompson, C. 2006, in Compact Stellar X-ray Sources, ed. W. H. G. Lewin & M. van der Klis (UK: Cambridge University Press)

Zhu, W., Kaspi, V. M., Dib, R., Woods, P. M., Gavriil, F. P., & Archibald, A. M. 2008, ApJ, 686, 520

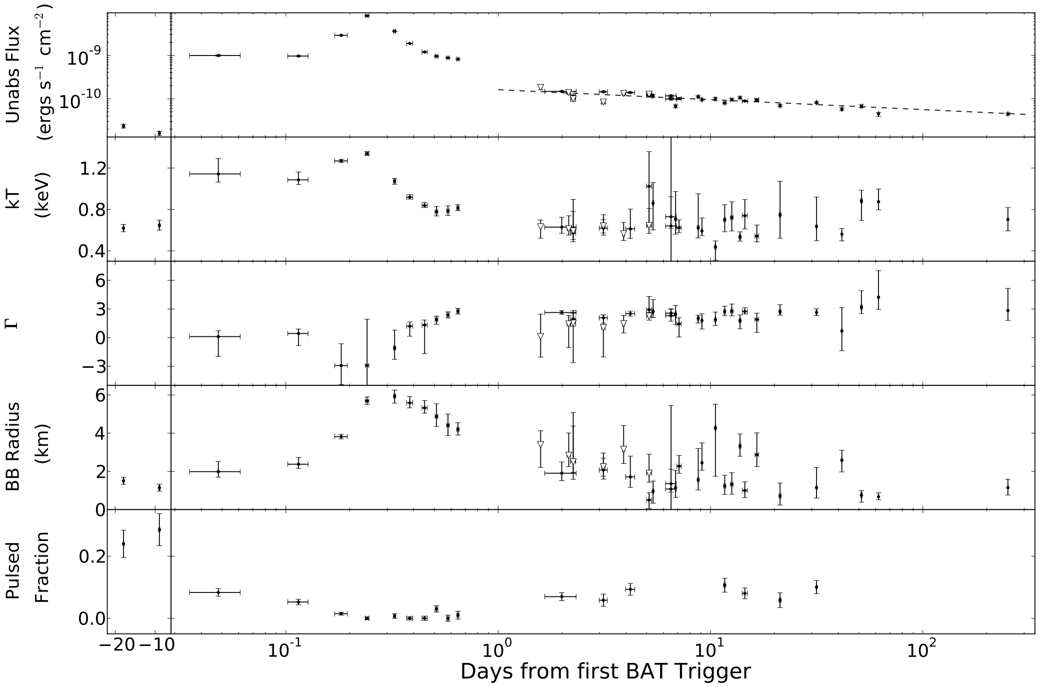

Figure 1. Properties of the persistent emission of 1E 1547−5408 surrounding the 2009 outburst event. The panels on the left show the two observations that preceded the event, on a linear time scale. The right-side panels are the post-event observations and are plotted on a logarithmic time scale. The dashed line in the top panel shows the power-law decay fit to the unabsorbed flux. The unabsorbed flux in the top panel and the pulsed fraction in the bottom panel are for the 1–10 keV range. The first ten points (the first day) after the BAT trigger are contaminated by dust scattering and should thus be regarded with caution. Some of the early PC mode observations had background regions that were contaminated by the dust scattering; these are marked with an open triangle.

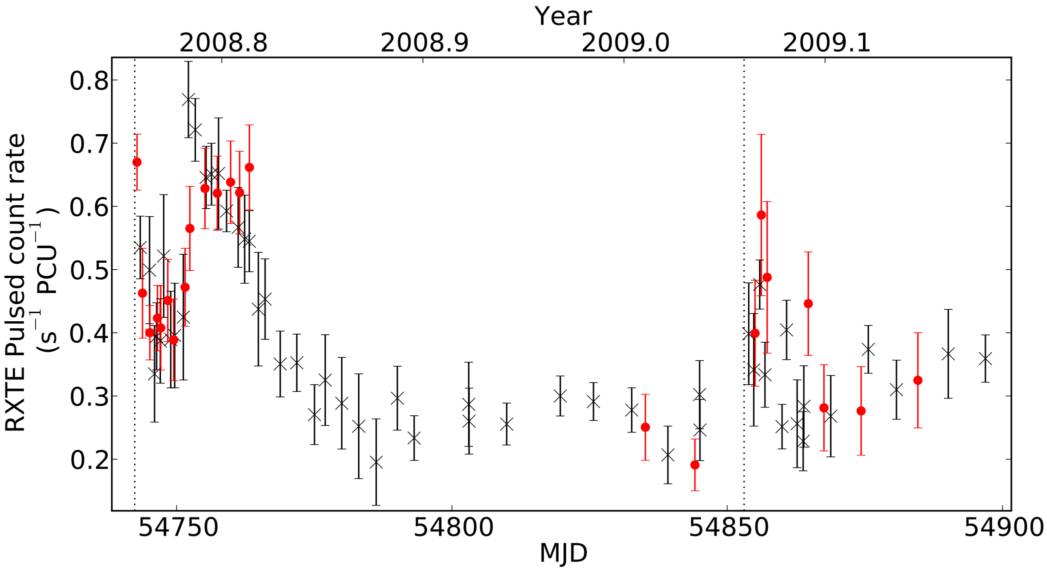

Figure 2. 2-10 keV RMS pulsed flux evolution of 1E 1547−5408 determined from *Swift* XRT and *RXTE*. The black crosses show the *RXTE* pulsed count rates and the red points are the *Swift* pulsed count rates, arbitrarily scaled to the *RXTE* values. The dotted vertical lines mark the onsets of the 2008 and 2009 outbursts.

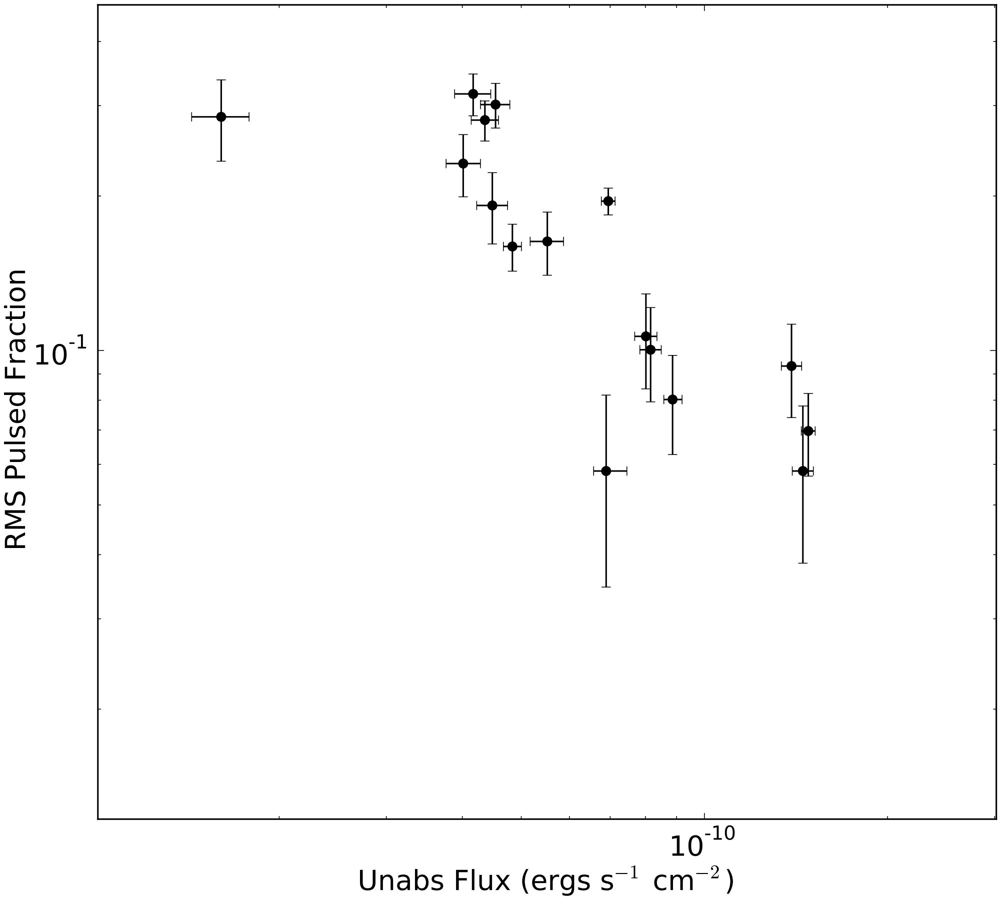

Figure 3. 1-10 keV RMS pulsed fraction as a function of 1-10 keV unabsorbed flux. See also Ng et al. (2011).

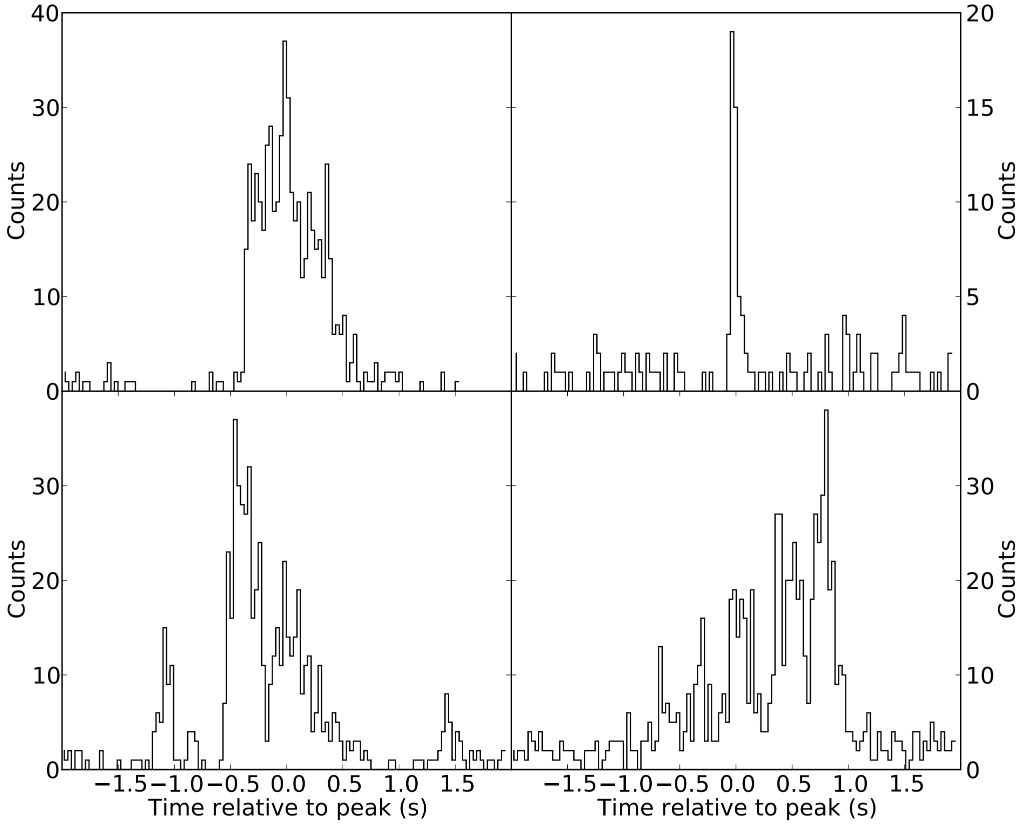

Figure 4. Examples of bursts from 1E 1547−5408. Time series are binned on a 1/16 s timescale in the 0.5–10 keV energy range. They display a wide range of morphology.

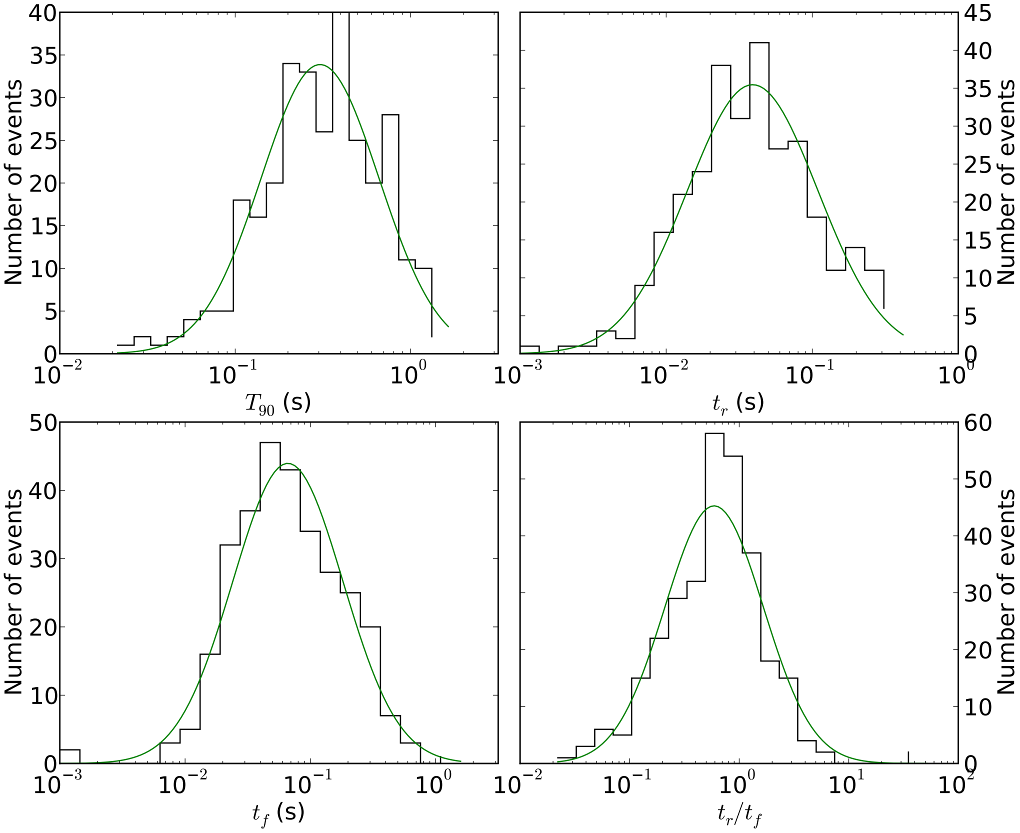

Figure 5. *Top left:* Distribution of T_{90} duration of bursts. *Top right:* Distribution of burst rise times. *Bottom left:* Distribution of burst fall times. *Bottom right:* Distribution of t_r/t_f. In all panels, the solid line is the best-fit log-normal function.

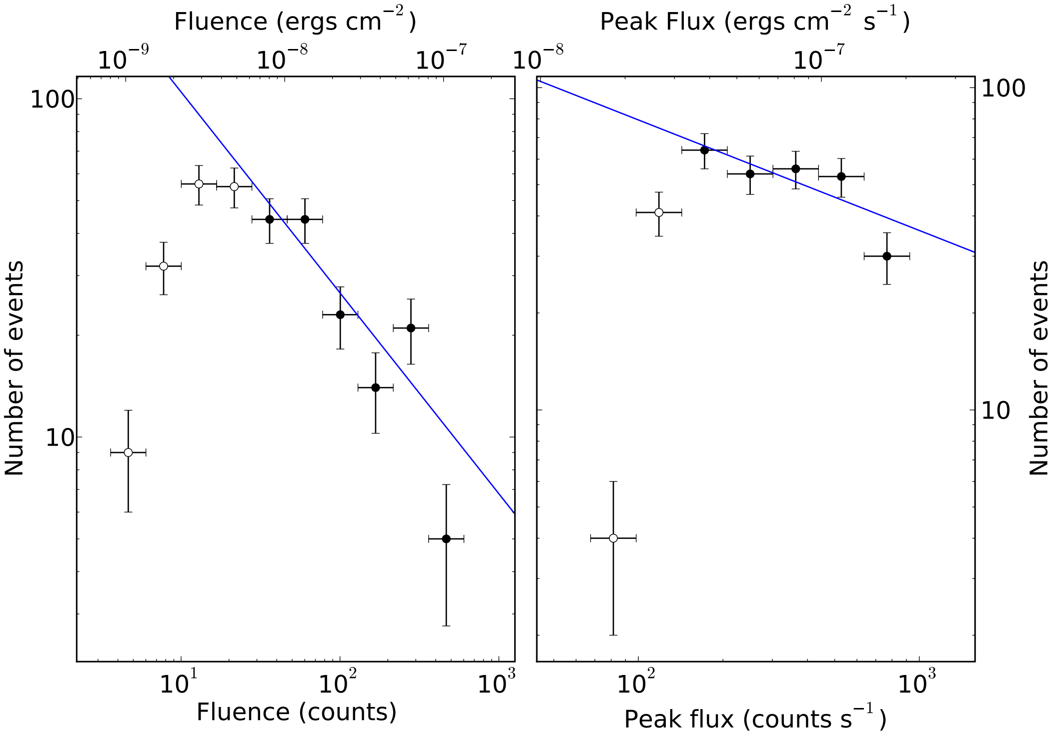

Figure 6. *Left:* Distribution of burst fluences. *Right:* Distribution of burst peak fluxes. The solid line is a linear fit to the filled circles. These distributions are based on burst counts from a 1–10 keV energy band. The open circles are not included in the fits because of reduced sensitivity in detecting such bursts. The top axes show the fluence and peak flux in cgs units which are derived from a single conversion factor between counts and ergs cm^{-2}. In using such a factor, the bursts are assumed to have the same spectrum which is an approximation as each burst has a slightly different spectrum.

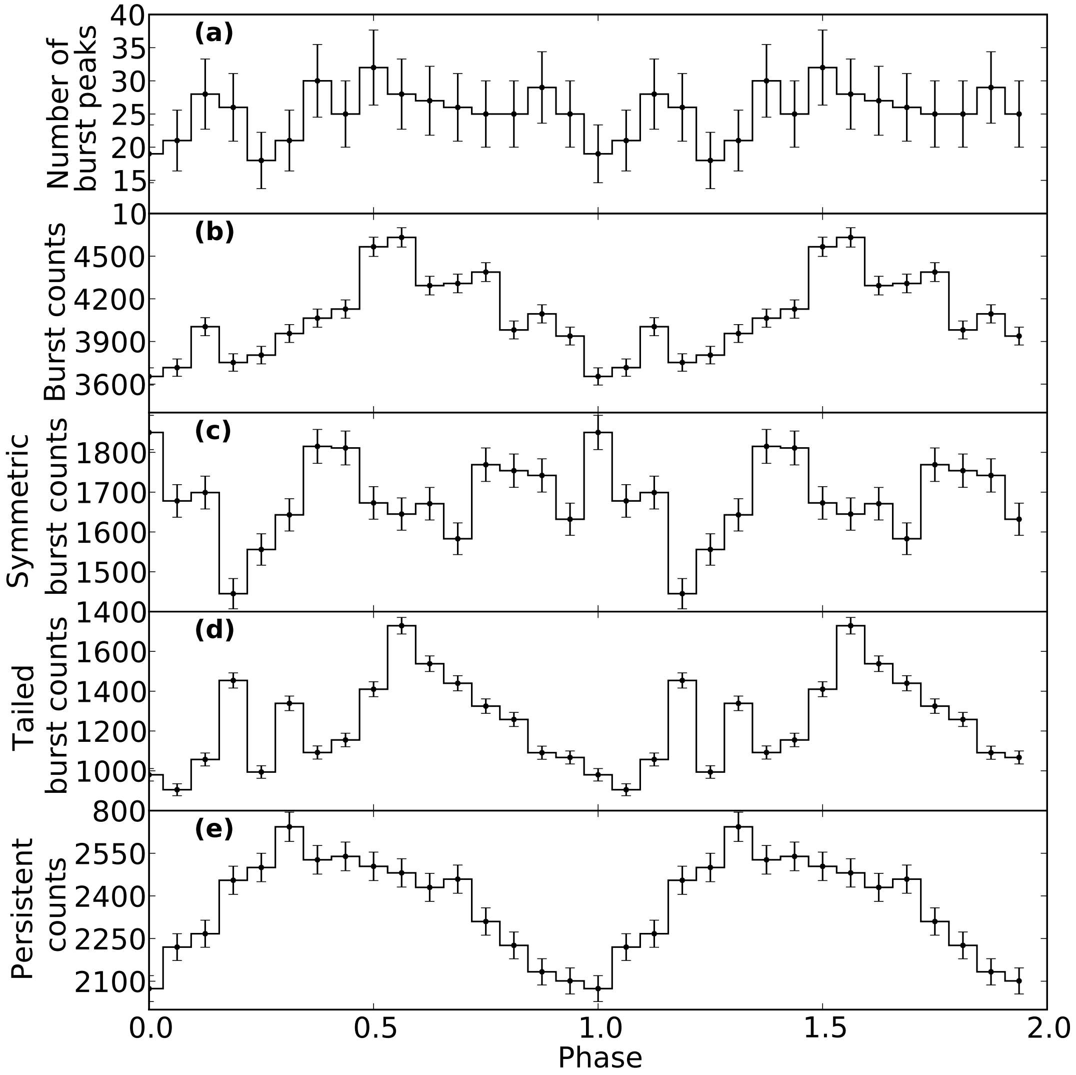

Figure 7. (a) Folded profile of the times of the burst peaks. (b) Folded profile of photon counts from cycles of the pulsar that contain bursts. (c) Folded profile of photon counts from cycles containing symmetric bursts. (d) Folded profile of photon counts from cycles containing slow-fall bursts. (e) Folded profile of photon counts from cycles of the pulsar that do not contain bursts but not including the first two observations following the BAT trigger, illustrating the quiescent pulse profile. Profiles are all in the 0.5–10 keV energy range.

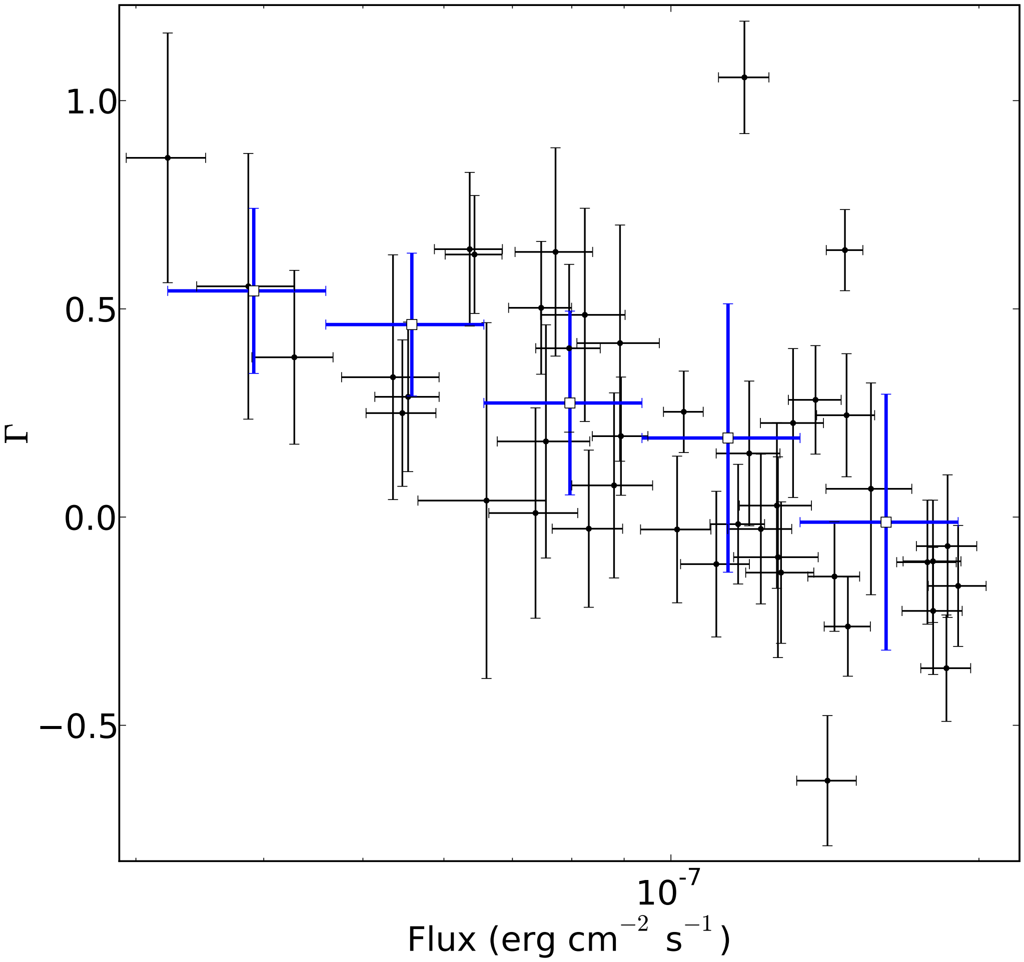

Figure 8. Power-law index as a function of average absorbed flux over T_{90} from the spectral fits of the 46 most fluent bursts. The black points are the individual bursts and the blue open squares represent the weighted averages of the power-law indices for bursts in logarithmic fluence bins.

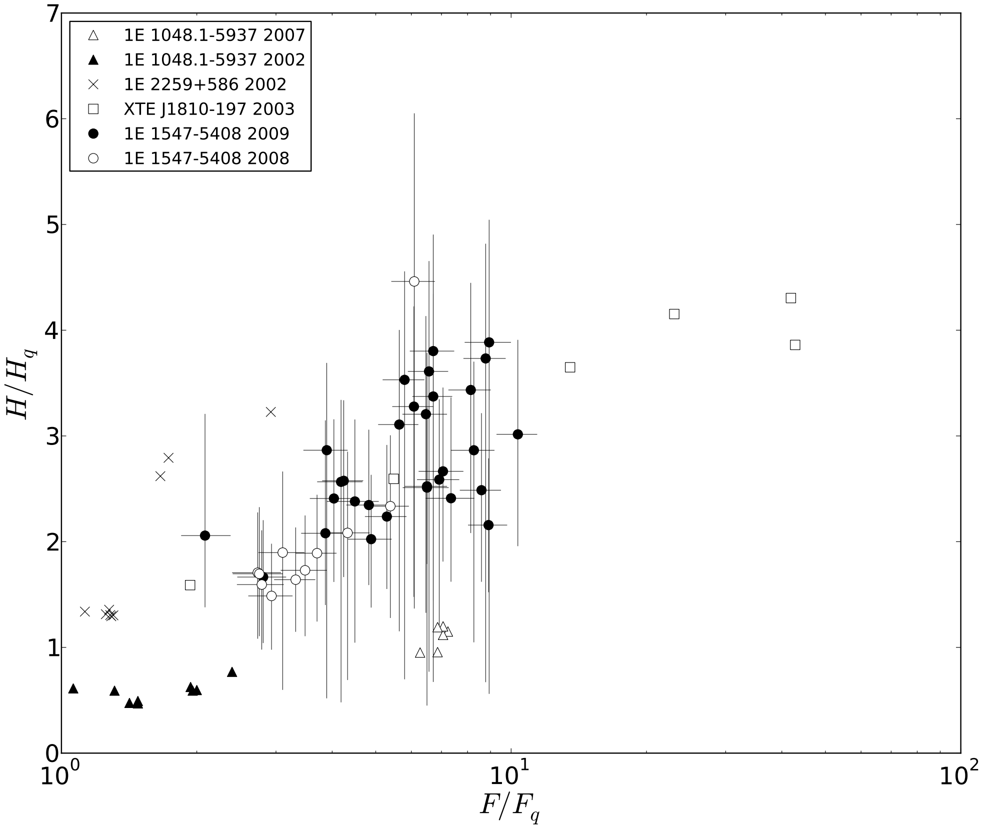

Figure 9. 4–10 keV / 2–4 keV flux hardness, H, as a function of 2–10 keV flux, F for magnetar outbursts. Both are normalised to their quiescent values, H_q, F_q. For 1E 1547−5408, the spectral fits used to determine the hardnesses and fluxes were from this work, and the first day of the 2009 outburst has been omitted due to contamination by the dust-scattered emission. For XTE J1810−197 the spectral parameters were taken from Gotthelf & Halpern (2007). For 1E 1048.1−5937 they were taken from Tam et al. (2008). For 1E 2259+586 they were taken from Zhu et al. (2008). Uncertainties on the hardness ratios are shown only for 1E 1547−5408; determining those for other sources is difficult from the literature, however they are likely comparable to the scatter.